ORIGINAL ARTICLE

A new method for apparent diffusion coefficient measurement using sequential ^{18}F-FDG PET and MRI: correlation with histological grade of invasive ductal carcinoma of the breast

Byung Hyun Byun · Woo Chul Noh · Ilhan Lim · Seung Sook Lee ·
A. Ra Cho · Ji Ae Park · Kyeong Min Kim · Hyun-Ah Kim · Eun-Kyu Kim ·
Byung Il Kim · Chang Woon Choi · Sang Moo Lim

Abstract

Objective The aim of this study was to measure the apparent diffusion coefficient (ADC) value at the region with the highest FDG uptake using sequential ^{18}F-FDG PET and MRI, and to correlate it with the histological grade of invasive ductal carcinoma (IDC) of the breast.

Methods A retrospective study was conducted on 75 untreated patients with IDC. First, a PET/CT scan and subsequent breast MRI were done and the SUV_{max} of the each breast tumor was recorded. Then, a PET image and ADC map were co-registered. On the axial slice containing the pixel with SUV_{max}, we drew multiple circular ROIs

within the tumor and measured the mean ADC value of each ROI. The average (ADC-mean) and minimum (ADC-min) of the mean ADC values for all ROIs within the tumor were calculated, respectively. Then, a circular ROI was placed at the corresponding location to the pixel with the highest SUV and the mean ADC value of the ROI was denoted as ADC-PET. We compared the averages of the ADC parameters and assessed the correlations among SUV_{max} and ADC parameters. ROC curve and logistic regression analyses were performed to assess the utility of ADC and SUV_{max} for detecting histological grade 3.

Results ADC-min was significantly lower than the ADC-mean or ADC-PET. All of the ADC parameters showed a negative correlation with SUV_{max}. The area under the ROC curve for identifying histological grade 3 using ADC-PET, ADC-min, ADC-mean and SUV_{max} was 0.684, 0.660, 0.633 and 0.639, respectively. By multivariate analysis, ADC-PET was a significant, independent predictor of histological grade 3 ($p = 0.004$).

Conclusions We estimated the ADC value at the breast tumor region with the highest FDG uptake using sequential ^{18}F-FDG PET and MRI. This new ADC parameter distinguished high-grade IDC, supporting the feasibility of the combined PET-MRI system in patients with breast cancer.

Keywords ADC · PET-MRI · Breast cancer · Histological grade

B. H. Byun · I. Lim · B. I. Kim · C. W. Choi · S. M. Lim (✉)
Department of Nuclear Medicine, Korea Cancer Center Hospital, Korea Institute of Radiological and Medical Sciences (KIRAMS), 75 Nowongil, Nowon Gu, Seoul 139-706, Republic of Korea
e-mail: smlim328@kcch.re.kr

B. H. Byun · I. Lim · J. A. Park · K. M. Kim ·
B. I. Kim · C. W. Choi · S. M. Lim
Molecular Imaging Research Center, Korea Institute of Radiological and Medical Sciences (KIRAMS), Seoul, Republic of Korea

W. C. Noh · H.-A. Kim · E.-K. Kim
Department of Surgery, Korea Cancer Center Hospital, Korea Institute of Radiological and Medical Sciences (KIRAMS), Seoul, Republic of Korea

S. S. Lee
Department of Pathology, Korea Cancer Center Hospital, Korea Institute of Radiological and Medical Sciences (KIRAMS), Seoul, Republic of Korea

A. R. Cho
Department of Nuclear Medicine, Seoul Medical Center, Seoul, Republic of Korea

Introduction

Diffusion-weighted MR image (DWI) represents in vivo images of biological tissues weighted with the local microstructural characteristics of water diffusion. The apparent diffusion coefficient (ADC) is used to quantify

water diffusion and tends to decrease in highly cellular tissue such as malignant tumors [1]. It has been reported that the ADC value is useful for differentiating benign from malignant breast masses [2] and correlates with prognostic factors in breast cancer [1–3]. However, the methods for measuring ADC, especially the locations for ADC measurements differ among these studies and there is no standard method to measure the ADC value. Hence it is necessary to normalize the location for ADC measurements across patients.

The degree of FDG uptake has been reported to positively correlate with the histological grade of breast cancer [4–6] based on the increased glucose utilization of malignant cells, and can be quantified and measured readily on ^{18}F-FDG PET/CT. The recently introduced combined PET-MRI system allows simultaneous [7, 8] or sequential acquisition [9] of PET and MRI images and there have been several literatures on integrated PET-MRI in the oncologic application [10, 11]. The aim of this study was to evaluate the feasibility of ADC measurements at the tumor region with the highest FDG uptake compared to the previously characterized methods [1–3] in patients with invasive ductal carcinoma (IDC) of the breast.

Materials and methods

Patient eligibility

A total of 173 consecutive patients with newly diagnosed, histopathologically proven IDC of the breast were registered between August 2008 and November 2011. All patients underwent sequential ^{18}F-FDG PET and MRI and subsequent mastectomy or breast-conserving surgery within a week. Subjects who had been treated with neo-adjuvant chemotherapy ($n = 91$), patients with a non-mass-like enhancement lesion on dynamic contrast-enhanced magnetic resonance imaging (DCE-MRI, $n = 6$) and one patient with a movement artifact on DWI were excluded, and as a result, a total of 75 patients were included in this retrospective study.

The enhancing solid tumor with the largest diameter on DCE-MRI was selected for analysis in each patient. Although the largest tumor for 3 of 75 patients was less than 1.0 cm (0.7–0.8 cm), all of these tumors were recognized on the ADC maps. As a result, a total of 75 tumors for 75 IDC patients were analyzed in the present study. This study was approved by our institutional review board. All patients provided written informed consent, and this study was performed according to the ethical guidelines of our institutional clinical research committee.

Imaging protocol of sequential ^{18}F-FDG PET and MRI

The whole-body PET/CT scanner (Biograph6; Siemens Medical Solutions, Malvern, PA, USA) was placed parallel to the 3.0-T whole-body MRI scanner (MAGNETOM Trio A Tim; Siemens Medical Solutions, Erlangen, Germany). These two scanners were located 10 m apart separated by an anti-magnetic wall.

The PET/CT imaging from skull base to the upper thigh (6–7 bed positions) was performed 60 min after ^{18}F-FDG injection, and this was followed by the breast MRI imaging. Both PET/CT and MRI images were acquired in a prone position and all patients moved from the PET/CT scanner to the MRI scanner (on independent patient tables) by walking. A dedicated positioning device which allows the same patient geometry as the breast MRI coil was used for PET/CT scan. Then, the breast PET and breast ADC maps were co-registered automatically using syngo Fused Vision 3D software (Siemens Medical Solutions, Erlangen, Germany) [12] and the agreements of contours of either breast mass or normal breast were visually assessed (acceptable vs. non-acceptable) independently by two observers. In 6 of 75 cases assessed as non-acceptable by any of two reviewers, PET and ADC maps were adjusted manually by consensus.

^{18}F-FDG PET/CT acquisition

All patients fasted for at least 6 h before intravenous administration of 7.4 MBq/kg of body weight of ^{18}F-FDG, which was produced in house using a 50-MeV cyslotron (MC-50; Scanditronix, Sweden) and a fully automated FDG synthesis module (TRACERlab MX; GE Healthcare, Germany). The specific activity and radiochemical purity of ^{18}F-FDG was >37 GBq/μmol and >98 %, respectively. Blood glucose levels did not exceed 7.2 mmol/L in any patient. Immediately, after the CT acquisition without intravenous iodinated contrast, PET data were acquired in the same anatomic locations, with a 16.2 cm axial field of view in 3D mode at 210 s/bed position (six to seven bed positions for each patient). CT scans were obtained using a 6-slice helical CT scanner and the imaging parameters used for CT scans were as follows: 130 kVp, 30 mA, 0.6 s/CT rotation, and a pitch of 6. The CT data were used for attenuation correction, and the images were reconstructed using a conventional iterative algorithm (ordered-subsets expectation–maximization, 2 iterations and 8 subsets).

MRI acquisition

MRI images were acquired using a 3.0-T whole-body MRI scanner with a dedicated phased-array breast coil. Before the administration of contrast agent, a T2-turbo spin-echo

sequence with fat suppression was performed. Diffusion-weighted images were acquired using a spin-echo type single-shot echo-planner imaging sequence. The parameters used were as follows: TR/TE 6100/78 ms; field of view 380 mm; matrix size 100 × 128; slice thickness 4 mm; receiver bandwidth 3004 Hz/pixel; and acquisition time 4 min 22 s. Imaging was performed with b values of 0 and 800 s/mm^2. Diffusion images were integrated in the three orthogonal directions to calculate the ADC maps. DCE-MRI images were also obtained using a three-dimensional (3D) fat suppressed volumetric interpolated breath hold examination (VIBE) sequence with parallel acquisition for one pre-contrast and five post-contrast dynamic series at 78, 144, 210, 300 and 366 s after contrast enhancement using TR/TE 3.95/1.49 ms; flip angle 10°; field of view 340 mm; matrix size 318 × 448; slice thickness 1 mm; 1 average; and the acquisition time of 7 min 19 s. The contrast agent, Gd-DTPA-BMA, (generic name : gadodiamide, Omniscan, GE Healthcare), was injected intravenously as a bolus (0.1 mmol/kg) at a rate of 1.5 mL/s using a power injector and this was followed by a 20 mL saline flush.

Image analysis

Automatically or manually co-registered PET and ADC maps were reviewed on the e-soft workstations (Simens Medical Systems, Iselin, NJ, USA). We drew an ellipsoid volume of interest including the breast tumor and adjacent breast tissue and measured the maximum standardized uptake value (SUV$_{max}$) on the PET/CT scan.

The average and minimum ADC value within the breast tumor were acquired on the breast MRI [10]. We selected an axial slice with the largest tumor diameter from the ADC map, and placed as many multiple circular ROIs of 25 mm^2 (with the diameter of about 5.6 mm) as possible within the tumor by referring to the enhancing solid portion of DCE-MRI. We did not test the registration error of DWI and PET images in the current study. To the best of our knowledge, there has been no report on the registration error of DWI and PET breast images using syngo Fused Vision 3D software. However, several researchers have reported that the automated registration of breast MRI and PET images resulted in the alignments of the breast within 4–6 mm accuracy [13–15], which is similar to the resolution of the our PET system (∼6 mm). Based on these reports, we speculated that the optimal diameter of ROI for ADC measurements in the current study would be 6 mm because a smaller ROI might be significantly influenced by the registration error and a larger ROI might contain more artifacts. Hence we adopted circular ROIs of 25 mm^2 with the diameter of about 5.6 mm, which is the closest diameter to the 6 mm in our system. The ROIs were carefully placed inside the tumor avoiding the cystic portion or visual

artifact, and the mean ADC values within each ROI were recorded. We calculated the average of the mean ADC values for all ROIs within the tumor (ADC-mean). Then, the ROI with the lowest mean ADC value within the tumor was selected and that ADC value was denoted as ADC-min (Fig. 1 a–c). PET and ADC maps were co-registered and the axial slice containing the pixel with the highest SUV was selected by adjusting the window of PET. A circular ROI of 25 mm^2 was placed at the nearest corresponding location to the pixel with the highest SUV avoiding the cystic portion or visual artifact. Then, the mean ADC value of the ROI was denoted as ADC-PET (Fig. 1 d–f).

Co-registered PET and ADC maps were independently reviewed by two of the authors. The ADC parameter measurements of each lesion were averaged for the two observers. When these 2 reviewers found an ADC discrepancy of more than 10 %, images were reviewed simultaneously and decisions were made by consensus.

Histological analysis

Tumor size was taken to be the largest diameter as determined on the gross specimen. Histological grades of IDC were assessed on the postsurgical specimen using a numerical scoring system (1, 2 and 3) for tubule formation, pleomorphism and mitotic count [16]. The total score ranges from 3 to 9: grade 1 represents a total score of 3–5, grade 2 represents a total score of 6 or 7 and grade 3 represents a total score of 8 or 9.

Statistical analysis

We presented statistics as the frequencies and percentages for categorical variables or as the mean ± standard deviation (SD) for normally distributed continuous variables or as the median [interquartile range (IQR)] for non-normally distributed continuous variables. All continuous variables were tested for normal distribution using the Shapiro–Wilk test. We compared the mean values of three ADC parameters (ADC-mean, ADC-min and ADC–PET) for all patients using the unpaired t test. The correlations among PET and MRI parameters (SUV$_{max}$, ADC-mean, ADC-min and ADC-PET) were assessed by using the Pearson's correlation test. The Mann–Whitney U test was used to compare the median values of the PET and MRI parameters associated with histological grades (grade 1 and 2 vs. grade 3). On the basis of the receiver operating characteristic (ROC) curve analysis, the optimal criteria of PET and MRI parameters that offered the highest sum of sensitivity and specificity for predicting histological grade 3 were, respectively, determined. The statistical significance of the difference among the areas under four ROC curves (95 % confidence intervals) was calculated by the method of Hanley and McNeil [17]. Then,
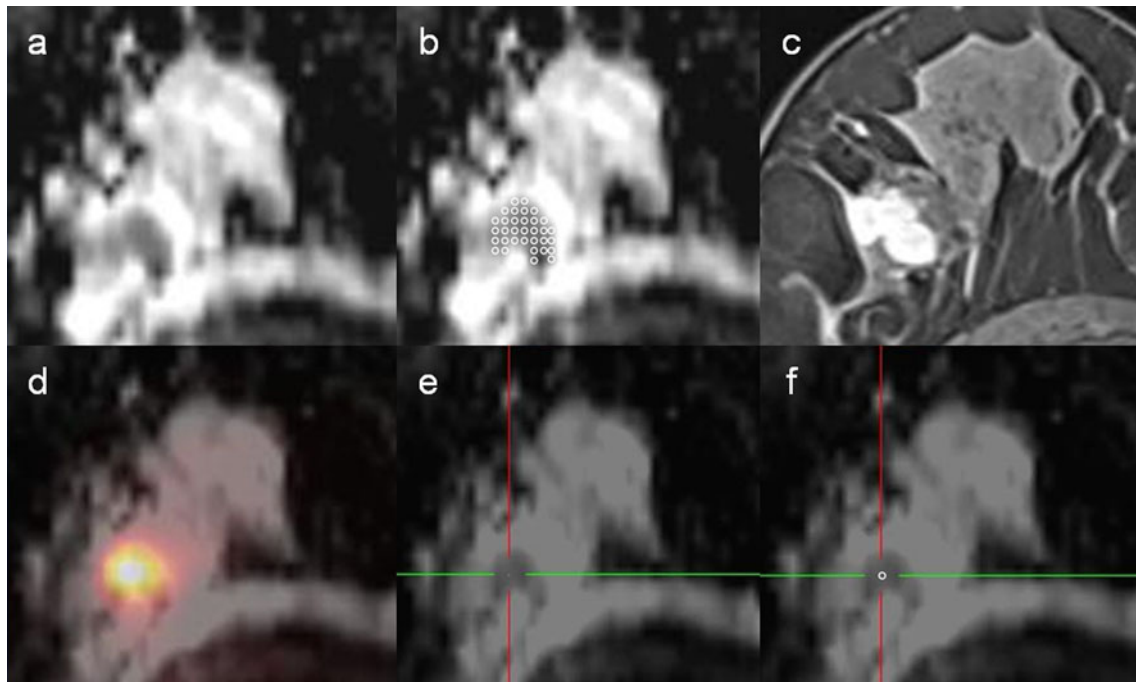
Fig. 1 Apparent diffusion coefficient (ADC) values within the mass lesion were measured by referring to DCE-MRI (**a–c**) and the co-registered image of PET and the ADC map (**d–f**). An axial slice with the largest tumor was selected from the ADC map (**a**), and multiple circular ROIs of 25 mm^2 were placed within the tumor on the ADC map (**b**) by referring to the enhancing solid portion of DCE-MRI (**c**). FDG PET and ADC maps were co-registered (**d**) and the axial slice containing the pixel with the highest SUV was selected by adjusting the window of FDG PET (**e**). Then, the mean ADC value of a circular ROI of 25 mm^2 on the corresponding location was denoted as ADC-PET (**f**)

we determined the most effective predictor among three ADC parameters by analysis of the area under the ROC curve. To compare the predictive value of this ADC parameter with those of SUV$_{max}$, age and tumor size, univariate and multivariate logistic regression was performed as follows: ADC and SUV$_{max}$ as dichotomous independent variables (above vs. below the optimal cutoff value determined by ROC analysis), age as a continuous independent variable, tumor size as a dichotomous independent variable (above vs. below median value) and histological grade as a dichotomous dependent variable (histological grade 1 or 2 vs. grade 3). Inter-observer agreements of ADC measurements were evaluated using both intraclass correlation coefficient (ICC) and Bland–Altman plots [18]. The statistical tests were performed using SPSS (version 13.0; SPSS Inc.) and MedCalc (MedCalc Software). All *p*-values were two-sided and statistical significance was accepted for *p*-values of <0.05.

Results

Patients characteristic

A total of 75 eligible female patients (mean age, 49.3 ± 8.8 years, range 24–37 years) comprising 6 patients (8 %) with histological grade 1, 24 patients (32 %) with histological grade 2, and 45 patients (60 %) with histological grade 3 were enrolled in this study. The mean values of tumor size and SUV$_{max}$ were 2.4 ± 1.4 and 6.0 ± 3.7 cm, respectively. The mean values of ADC-mean, ADC-min, and ADC-PET were $1.179 ± 0.308 × 10^{-3}$ mm^2/s, $1.040 ± 0.226 × 10^{-3}$ mm^2/s, and $1.141 ± 0.324 × 10^{-3}$ mm^2/s, respectively. The ADC-min was significantly lower than the ADC-mean or ADC-PET ($p < 0.001$, $p = 0.027$, respectively). However, there was no significant difference between the ADC-mean and ADC-PET ($p = 0.198$).

Correlations among PET and MRI parameters

Figure 2 shows the relationships between SUV$_{max}$ and ADC parameters. The ADC-mean and ADC-min showed a significant negative correlation with SUVmax ($r = -0.229$, $p = 0.048$ and $r = -0.267$, $p = 0.021$, respectively) and ADC-PET showed a marginally significant negative correlation with SUV$_{max}$ ($r = -0.222$, $p = 0.056$).

Figure 3 shows the relationships among three ADC parameters. ADC-mean and ADC-min ($r = 0.898$, $p < 0.001$), ADC-mean and ADC-PET ($r = 0.910$, $p < 0.001$) and ADC-min and ADC-PET ($r = 0.878$, $p < 0.001$) had strong positive correlations with each other.
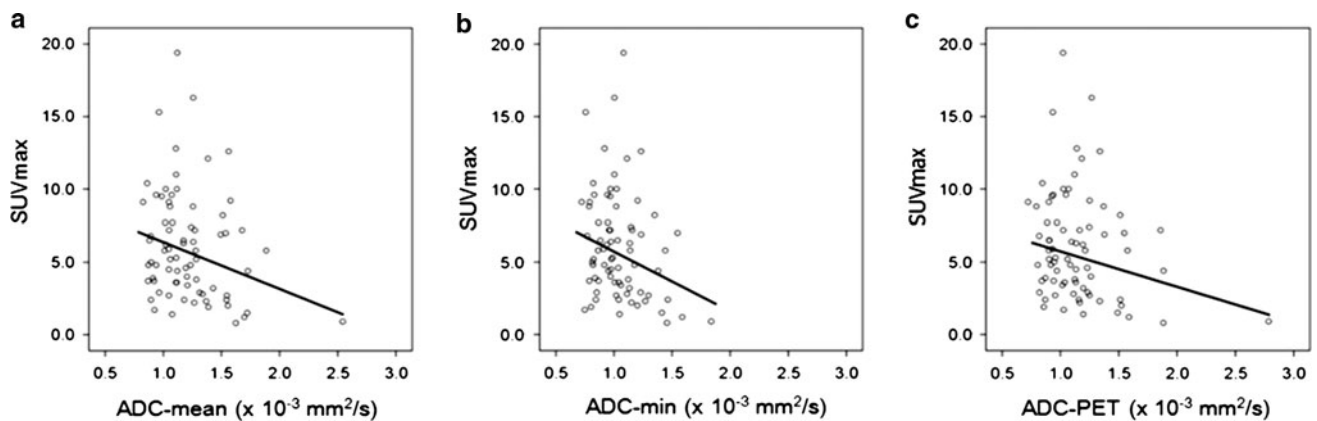
Fig. 2 Relationships between ADC-mean and SUV$_{max}$ ($r = -0.229$, $p = 0.048$) (**a**), ADC-min and SUV$_{max}$ ($r = -0.267$, $p = 0.021$) (**b**), and ADC-PET and SUV$_{max}$ ($r = -0.222$, $p = 0.056$) (**c**)
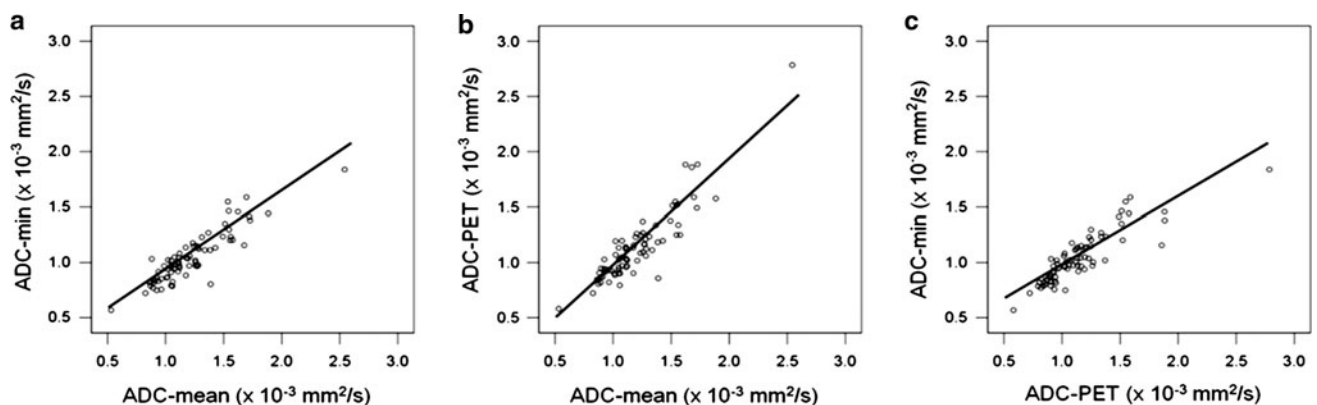

Fig. 3 Relationship between ADC-mean and ADC-min ($r = 0.898$, $p < 0.001$) (**a**), ADC-mean and ADC-PET ($r = 0.910$, $p < 0.001$) (**b**), and ADC-PET and ADC-min ($r = 0.878$, $p < 0.001$) (**c**)

PET and MRI parameters according to histological grade

There were statistically significant differences between histological grade 3 and others for PET and MRI parameters (SUV$_{max}$, ADC-min and ADC-PET, $p < 0.050$ for all comparisons) except for ADC-mean ($p = 0.056$; Table 1). The SUV$_{max}$ of histological grade 3 tumors was significantly higher than that of grade 1 or 2 tumors. On the other hand, ADC-min and ADC-PET of histological grade 3 tumors were significantly lower than those of grade 1 or 2 tumors.

Predictive values of PET and MRI parameters

On the ROC curve analysis for discriminating histological grade 3 from grade 1 or 2, ADC-PET showed the highest area under the curve 0.684 (95 % CI 0.567–0.787). The areas under the curve of ADC-min, ADC-mean and SUV$_{max}$ were 0.660 (95 % CI 0.542–0.766), 0.633 (95 % CI 0.513–0.741) and 0.639 (95 % CI 0.520–0.747),

respectively (Fig. 4). There were no statistically significant differences among the areas under the curve of these four parameters ($p > 0.10$ for all comparisons). The optimal cutoff values for ADC-PET, ADC-min, ADC-mean and SUV$_{max}$ were 1.095, 1.037, 1.077 and 4.5 with the sensitivity/specificity for detecting high-grade IDC of 68.9 %/76.7 %, 73.3 %/63.3 %, 53.3 %/73.3 % and 71.1 %/56.7 %, respectively. From these results, ADC-PET was used as the most effective predictor among three ADC parameters in the prediction of histological grade 3.

In the univariate analysis, tumor size, SUV$_{max}$ and ADC-PET were significant predictors for histological grade 3. However, in the multivariate analysis, only tumor size and ADC-PET were determined to be significant (Table 2).

Interobserver agreements of ADC Values

The ICCs for ADC-PET, ADC-min, and ADC-mean were 0.980 (95 % CI 0.970–0.987), 0.975 (95 % CI 0.961–0.984), and 0.913 (95 % CI 0.867–0.944),

Table 1 PET and MRI parameters stratified by histological grade

Parameter	Histological grade				p value*
	Grade 1 or 2 (n = 30)		Grade 3 (n = 45)		
	Median	IQR	Median	IQR	
SUV$_{max}$	4.0	2.4–6.7	5.9	3.8–9.1	0.042
ADC-mean, 10^{-3} mm^2/s	1.196	1.047–1.473	1.054	1.018–1.167	0.056
ADC-min, 10^{-3} mm^2/s	1.059	0.946–1.211	0.969	0.918–1.019	0.019
ADC-PET, 10^{-3} mm^2/s	1.165	1.041–1.319	1.024	0.940–1.078	0.007

IQR interquartile range

* p values show the statistical significance of the differences between the PET and MR parameters and histological grade, assessed by the Mann–Whitney *U* test

Fig. 4 Receiver operating characteristic curves to assess the utility of apparent diffusion coefficient (ADC) values and SUV$_{max}$ for discriminating histological grade 3 from grade 1 or 2. ADC-PET (**a**) shows a higher area under the curve compared to ADC-min (**b**), ADC-mean (**c**) or SUV$_{max}$ (**d**)
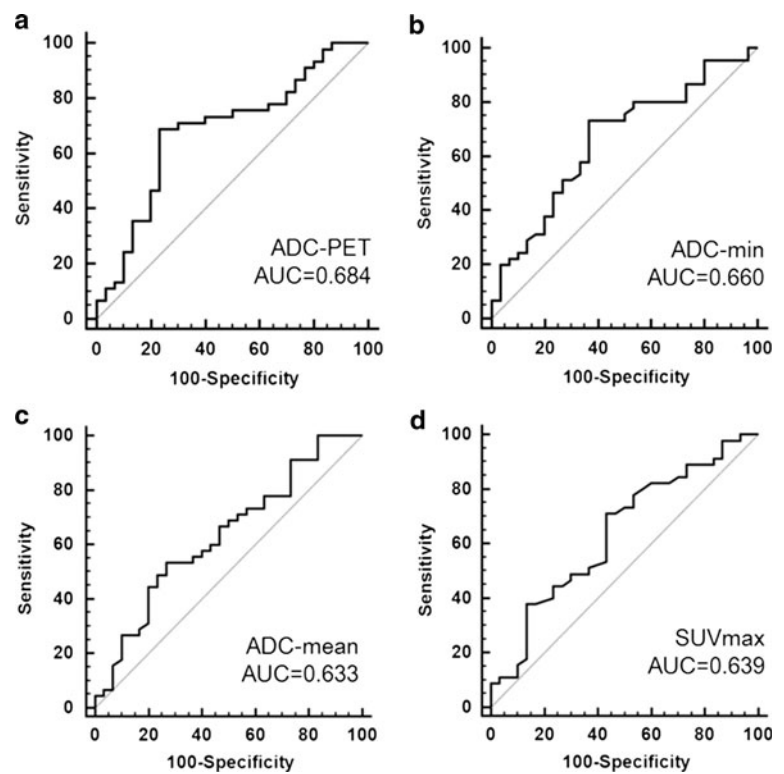
Table 2 Results of logistic regression analysis

Covariate	Univariate		Multivariate	
	Odd ratio (95 % CI)	p value	Odd ratio (95 % CI)	p value
Age (continuous variable)	1.002 (0.950–1.058)	0.930	Not included	
Tumor size (>2.2 cm vs. others)	6.089 (2.182–16.992)	0.001	5.333 (1.783–15.954)	0.003
SUV$_{max}$ (>4.5 vs. others)	3.219 (1.223–8.474)	0.018		0.236
ADC-PET (<1.095 vs. others)	5.955 (2.098–16.904)	0.001	5.195 (1.701–15.864)	0.004

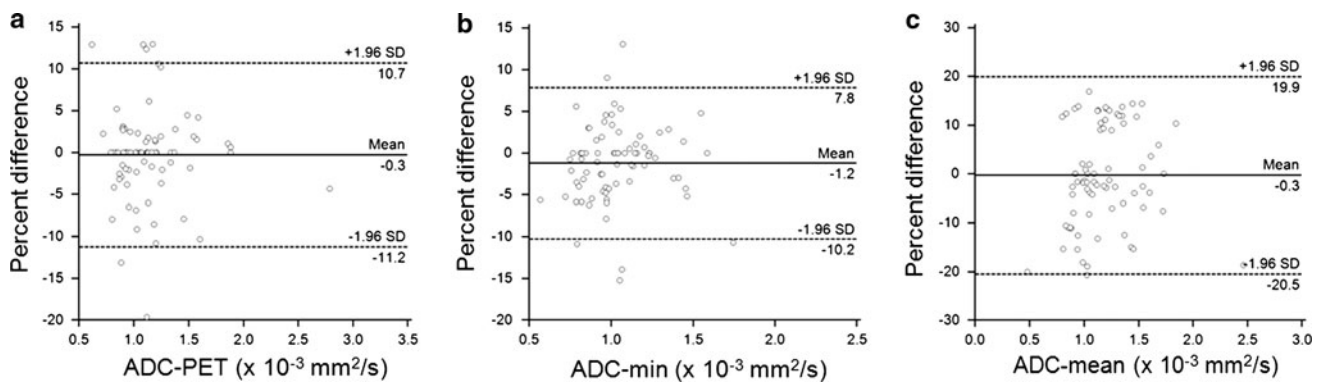Dependent variable was histological grade with grouping 1 and 2 vs. 3

Fig. 5 Bland–Altman plots representing interobserver bias and agreement regarding ADC-PET (**a**), ADC-min (**b**), and ADC-mean (**c**) by 2 observers. The mean difference (*solid line*) and 95 % limits of agreement intervals (*dashed lines*) are also shown

respectively. Corresponding Bland–Altman plots are depicted in Fig. 5.

Discussion

It has been demonstrated that the tumors with high glucose metabolism or high histological grade proliferate actively [19], and increased FDG uptake of primary breast cancer is associated with higher histological grade [20, 21]. However, acute and chronic inflammation, benign breast masses, and postsurgical changes, may also show increased FDG uptake [22]. Besides, smaller tumors (less than 1 cm) and low-grade tumors have been reported to be associated with less FDG uptake (SUV less than 2.5), which results in a false negative FDG PET in patients with breast cancer [23].

It has been assumed that the decreased ADC value of malignant tumors is due to their increased cellularity, larger nuclei with more abundant macromolecular proteins, and reduced extracellular space [24, 25]. However, mastitis or inflammatory breast carcinoma may show a decreased ADC value [26]. Moreover, there is no standard of method for measuring the ADC value. Researchers have placed a ROI on the ADC maps as large as possible within the mass [27], around the central region of the mass [28], or selected the lowest ADC from the three ROIs placed at the most enhanced area of the mass [29], and yet, controversy still exists in the literature regarding the relationship between the ADC value and histological grade in patients with breast cancer [4, 6].

Recently, Hirano et al. [2] drew as many multiple ROIs of 25 mm^2 as possible within the 75 benign or malignant breast masses, then calculated the average, minimum, and maximum ADC values as well as the difference between the minimum and maximum ADC value in each tumor, respectively. They reported that the minimum ADC value was an optimal DWI single parameter for differentiation

between malignant and benign lesions of breast masses with both sensitivity and specificity of 85.5 %. By analyzing the histological specimen, they suggested that regions of minimum ADC reflected the highest cellular zone and the regions of maximum ADC reflected the lowest cellular zone. We also employed multiple ROIs of 25 mm^2 within the breast masses to calculate the ADC values, because a pixel-based measurement of minimum ADC value would be more susceptible to noise and misregistration. Nonetheless, the minimum ADC value among multiple ROIs within breast masses is still presumed to be the sum of the true ADC value and these artifacts may result in the over- or underestimation of the true ADC value. Moreover, this multiple ROI method is laborious and time-consuming and thus its applicability can be limited in clinical practice. It was much more convenient to measure ADC-PET than ADC-min or ADC-mean in the current study. The ICCs of ADC values were very high (>0.9) and the inter-observer 95 % limits of agreement were approximately ±10 % for ADC-min and ADC-PET, and ±20 % for ADC-mean, respectively. Based on these results, we speculate that the interobserver variability in the current study would not be as large as to affect our conclusion. Nonetheless, we can expect more reliable measurement of ADC-PET by using the simultaneous PET-MRI system.

It has been demonstrated that the degree of FDG uptake in breast cancer had a significant correlation with the proliferation index [30, 31]. We assumed that the pixel with the highest SUV represented the most actively proliferating region of breast cancer and hence, ADC-PET reflected the cellularity, size of nuclei, and the amount of extracellular space of that region, which might carry different information than conventional ADC parameters. It is supposed that the region with the highest SUV represents the most actively proliferating cancer cells rather than inflammatory cells. Therefore, we also expected to lower the chance of the ADC value representing inflammation or

artifact other than cancer cells by measuring ADC-PET. Besides different biological information, noise, misregistration, and concomitant inflammation might affect the significant difference between ADC-min and ADC-PET in the present study (1.040 vs. 1.141, mean, respectively).

A significant negative relationship ($p = 0.001$) between SUV_{max} and ADC of 44 breast cancers (9 ductal carcinoma in situ and 35 IDC) was reported by Nakajo et al. [8]. In the present larger-scale study ($n = 76$ vs. 44) with IDC, a significant or marginally significant correlation between SUV_{max} and ADC parameters were observed ($p = 0.021$–0.056). Although SUV_{max} and ADC parameters of breast cancers show a significant association with histological grade in both studies, the biological information of these parameters are different from each other (e.g. glucose metabolism and cellularity). Moreover, 45 of 75 patients (60 %) were categorized as histological grade 3 in our study compared with 10 of 44 (22 %) in their study. Further studies are warranted to define the relationship between the SUV and ADC parameters of breast cancers.

The ROC curve and logistic regression analysis in the present study show that ADC-PET is useful to discriminate high-grade IDC patients. These data indicate that the ADC value measured at the tumor region with the highest FDG uptake may provide useful biological information (e.g., cellularity of the most actively proliferating portion of malignant tumor), and support the feasibility for the simultaneous acquisition of PET and MRI in patients with breast cancer. Future works on the use of this new PET and MRI parameter together with SUV_{max}, a widely used metabolic parameter, for evaluating treatment response, tumor recurrence, and predicting prognosis in cancer patients will be required.

The present study has several limitations. First, the PET/CT and breast MRI images were not acquired simultaneously but sequentially. However, the breast MRI imaging was performed immediately after the PET/CT scan with the same position and dedicated positioning breast device, and the majority of these two images were automatically co-registered precisely so that the contours of breast masses or normal breasts were assessed to be identical. Nonetheless, manual adjustments were needed in several patients because of the inaccurate co-registration of PET/CT and MRI, probably due to the patient motion artifact [9]. The simultaneous PET-MRI system will allow less motion artifact and more reliable PET and MRI parameters. Second, we did not perform histological analysis of the corresponding region with the highest FDG uptake or lowest ADC parameters on the postsurgical specimen [5]. Studies with the histological analysis of these regions are needed to further confirm the usefulness of ADC-PET, the new PET and MRI parameter. Third, we did not analyze the risk of radiation exposure. Finally, we did not analyze the cost-effectiveness of these studies.

Conclusion

By using sequential ^{18}F-FDG PET and MRI, we can readily estimate the ADC value at the region with the highest FDG uptake of breast cancer and this new ADC parameter may be useful to discriminate high-grade breast cancer. These data support the feasibility of the combined PET-MRI system in patients with breast cancer.

References

1. Choi SY, Chang YW, Park HJ, Kim HJ, Hong SS, Seo DY. Correlation of diffusion-weighted imaging apparent diffusion coefficient with prognostic factors of breast cancer. Br J Radiol. 2012;85:e474–9.
2. Hirano M, Satake H, Ishigaki S, Ikeda M, Kawai H, Naganawa S. Diffusion-weighted imaging of breast masses: comparison of diagnostic performance using various apparent diffusion coefficient parameters. Am J Roentgenol. 2012;198:717–22.
3. Razek AA, Gaballa G, Denewer A, Nada N. Invasive ductal carcinoma: correlation of apparent diffusion coefficient value with pathological prognostic factors. NMR Biomed. 2010;23:619–23.
4. Oshida M, Uno K, Suzuki M, Nagashima T, Hashimoto H, Yagata H, et al. Predicting the prognoses of breast carcinoma patients with positron emission tomography using 2-deoxy-2-fluoro[18F]-D-glucose. Cancer. 1998;82:2227–34.
5. Inoue T, Yutani K, Taguchi T, Tamaki Y, Shiba E, Noguchi S. Preoperative evaluation of prognosis in breast cancer patients by [(18)F]2-deoxy-2-fluoro-D-glucose-positron emission tomography. J Cancer Res Clin Oncol. 2004;130:273–8.
6. Nakajo M, Kajiya Y, Kaneko T, Kaneko Y, Takasaki T, Tani A, et al. FDG PET/CT and diffusion-weighted imaging for breast cancer: prognostic value of maximum standardized uptake values and apparent diffusion coefficient values of the primary lesion. Eur J Nucl Med Mol Imaging. 2010;37:2011–20.
7. Drzezga A, Souvatzoglou M, Eiber M, Beer AJ, Fürst S, Martinez-Möller A, et al. First clinical experience with integrated whole-body PET/MR: comparison to PET/CT in patients with oncologic diagnoses. J Nucl Med. 2012;53:845–55.
8. Zaidi H, Ojha N, Morich M, Hu Z, Maniawski P, Ratib O, et al. Design and performance evaluation of a whole-body Ingenuity TF PET-MRI system. Phys Med Biol. 2011;56:3091–106.
9. Delso G, Ziegler S. PET/MRI system design. Eur J Nucl Med Mol Imaging. 2009;36(Suppl):S86–92.
10. Buchbender C, Heusner TA, Lauenstein TC, Bockisch A, Antoch G. Oncologic PET/MRI, part 1: tumors of the brain, head and neck, chest, abdomen, and pelvis. J Nucl Med. 2012;53:928–38.
11. Park H, Wood D, Hussain H, Meyer CR, Shah RB, Johnson TD, et al. Introducing parametric fusion PET/MRI of primary prostate cancer. J Nucl Med. 2012;53:546–51.
12. Hoppenrath M. Understanding multimodal fusion imaging. Appl Radiol. 2004;33:40–7.
13. Dmitriev ID, Loo CE, Vogel WV, Pengel KE, Gilhuijs KG. Fully automated deformable registration of breast DCE-MRI and PET/CT. Phys Med Biol. 2013;21:1221–33.

14. Unlu MZ, Krol A, Magri A, Mandel JA, Lee W, Baum KG, et al. Computerized method for nonrigid MR-to-PET breast-image registration. Comput Biol Med. 2010;40:37–53.

15. Kiefer A, Kuwert T, Hahn D, Hornegger J, Uder M, Ritt P. Anatomical accuracy of abdominal lesion localization. Retrospective automatic rigid image registration between FDG-PET and MRI. Nuklearmedizin. 2011;50:147–54.

16. Elston CW, Ellis IO. Pathological prognostic factors in breast cancer. I. The value of histological grade in breast cancer: experience from a large study with long-term follow-up. Histopathology. 1991;19:403–10.

17. Hanley JA, McNeil BJ. A method of comparing the areas under receiver operating characteristic curves derived from the same cases. Radiology. 1983;148:839–43.

18. Bland JM, Altman DG. Statistical methods for assessing agreement between two methods of clinical measurement. Lancet. 1986;1:307–10.

19. Avril N, Menzel M, Dose J, Schelling M, Weber W, Jänicke F, et al. Glucose metabolism of breast cancer assessed by 18F-FDG PET: histologic and immunohistochemical tissue analysis. J Nucl Med. 2001;42:9–16.

20. Gil-Rendo A, Martinez-Regueira F, Zornoza G, Garcia-Velloso MJ, Beorlegui C, Rodriguez-Spiteri N. Association between [18F]fluorodeoxyglucose uptake and prognostic parameters in breast cancer. Brit J surg. 2009;96:166–70.

21. Sanli Y, Kuyumcu S, Ozkan ZG, Işik G, Karanlik H, Guzelbey B, et al. Increased FDG uptake in breast cancer is associated with prognostic factors. Ann Nucl Med. 2012;26:345–50.

22. Adejolu M, Huo L, Rohren E, Santiago L, Yang WT. False-positive lesions mimicking breast cancer on FDG PET and PET/CT. Am J Roentgenol. 2012;198:W304–14.

23. Avril N, Rose CA, Schelling M, Dose J, Kuhn W, Bense S, et al. Breast imaging with positron emission tomography and fluorine-18 fluorodeoxyglucose: use and limitations. J Clin Oncol. 2000;18:3495–502.

24. Tsushima Y, Takahashi-Taketomi A, Endo K. Magnetic resonance (MR) differential diagnosis of breast tumors using apparent diffusion coefficient (ADC) on 1.5-T. J Magn Reson Imaging. 2009;30:249–55.

25. Humphries PD, Sebire NJ, Siegel MJ, Olsen OE. Tumors in pediatric patients at diffusion-weighted MR imaging: apparent diffusion coefficient and tumor cellularity. Radiology. 2007;245:848–54.

26. Kul S, Cansu A, Alhan E, Dinc H, Gunes G, Reis A. Contribution of diffusion-weighted imaging to dynamic contrast-enhanced MRI in the characterization of breast tumors. Am J Roentgenol. 2011;196:210–7.

27. Satake H, Nishio A, Ikeda M, Ishigaki S, Shimamoto K, Hirano M, et al. Predictive value for malignancy of suspicious breast masses of BI-RADS categories 4 and 5 using ultrasound elastography and MR diffusion-weighted imaging. Am J Roentgenol. 2011;196:202–9.

28. Rubesova E, Grell AS, De Maertelaer V, Metens T, Chao SL, Lemort M. Quantitative diffusion imaging in breast cancer: a clinical prospective study. J Magn Reson Imaging. 2006;24:319–24.

29. Yabuuchi H, Matsuo Y, Okafuji T, Kamitani T, Soeda H, Setoguchi T, et al. Enhanced mass on contrast-enhanced breast MR imaging: lesion characterization using combination of dynamic contrast-enhanced and diffusion-weighted MR images. J Magn Reson Imaging. 2008;28:1157–65.

30. Tchou J, Sonnad SS, Bergey MR, Basu S, Tomaszewski J, Alavi A, et al. Degree of tumor FDG uptake correlates with proliferation index in triple negative breast cancer. Mol Imaging Biol. 2010;12:657–62.

31. Shimoda W, Hayashi M, Murakami K, Oyama T, Sunagawa M. The relationship between FDG uptake in PET scans and biological behavior in breast cancer. Breast cancer. 2007;14:260–8.